Effect of Anion Ordering on the H-Anion Interactions and Band Electronic Structure of $(TMTSF)_2BF_4$ at 20 K

Thomas J. Emge,[†] Hau H. Wang,[†] Mark A. Beno,[†] Jack M. Williams,*[†] M.-H. Whangbo,*[‡] and M. Evain[‡§]

Contribution from the Chemistry and Materials Science Divisions, Argonne National Laboratory, Argonne, Illinois 60439, and Department of Chemistry, North Carolina State University, Raleigh, North Carolina 27695-8204. *Received May 9, 1986*

Abstract: Single crystal neutron diffraction studies were carried out for $(TMTSF)_2BF_4$ at 20 K to accurately determine the methyl group H atom positions of the TMTSF molecule. At 20 K, this salt has the $(2a \times 2b \times 2c)$ superstructure, with respect to the $(a \times b \times c)$ structure observed above its anion ordering temperature ~40 K. The structural features of the anion ordering were described in terms of short H···F contacts between BF_4^- anions and TMTSF molecules. Also, the anion ordering in $(TMTSF)_2BF_4$ is apparently independent of cooling rate, since the completely ordered superstructures obtained upon fast (~6 deg min^{-1}) and slow (~0.2 deg min^{-1}) cooling of the crystal to 20 K do not vary significantly. The nature of the metal-insulator transition in $(TMTSF)_2BF_4$, which is a consequence of the anion ordering, was studied by performing tight binding band calculations for the 125 and 20 K crystal structures of $(TMTSF)_2BF_4$. This salt is a narrow band gap (~0.1 eV) semiconductor at 20 K, which is a result of the Peierls distortion involving the half-filled valence band of $(TMTSF)_2BF_4$ above ~40 K.

Bis(tetramethyltetraselenafulvalenium) tetrafluoroborate, $(TMTSF)_2BF_4$ $[(C_{10}H_{12}Se_4)_2^+BF_4^-]$ belongs to the $(TMTSF)_2X$ family of organic conductors, where X^- is a monovalent anion (Bechgaard salts).[1] The $(TMTSF)_2X$ salts are *isostructural* at room temperature and are characterized by one-dimensional (1D) chains of interacting TMTSF radical cations.[2-5] As a result of the face-to-face stacking of TMTSF molecules along the crystallographic *a* axis, $(TMTSF)_2X$ salts show a 1D metallic electronic band[6,7] and anisotropic electrical conductivity.[1,8] The physical properties of these salts include metallic behavior,[8] superconductivity,[9,10] and metal-insulator (MI) transitions that occur after the onset of anion ordering (AO)[11-14] or spin-density wave formation (SDW).[15,16] The structural distortions that accompany the MI transitions in some $(TMTSF)_2X$ salts are Peierls-like,[17,18,47] in that the high temperature monomeric chains of TMTSF molecules become dimerized at a lower temperature, such that a gap is created in the electronic band at the Fermi level. This electronic transition is possible because the highest occupied band, which is half-filled and narrow,[6] is stabilized when split into the two bands (one filled, one empty) at temperatures below T_{MI}.

The variety of low-temperature properties that $(TMTSF)_2X$ organic metals exhibit are exemplified by the salts with $X^- = BF_4^-$, ReO_4^-, and ClO_4^-, which all undergo anion ordering at low temperature. All of the Bechgaard salts except $(TMTSF)_2ClO_4$ undergo MI transitions at low temperature.[1,8] Although $(TMTSF)_2BF_4$ is isostructural to $(TMTSF)_2ClO_4$ and the BF_4^- anion is only slightly smaller than ClO_4^-, anion ordering results in an MI transition for $(TMTSF)_2BF_4$ but not for $(TMTSF)_2ClO_4$. The detailed structures of these salts at temperatures below T_{MI}, in particular their different intermolecular interaction geometries that result from their different anion sizes, will aid in the understanding of their structure-property relationships. The crystallographic transitions associated with anion ordering in $(TMTSF)_2BF_4$[22] (40 K) and $(TMTSF)_2ReO_4$[11,23,24] (180 K) are of the same form (i.e., their unit cells transform from $a \times b \times c$, space group $P\bar{1}$, to $2a \times 2b \times 2c$, space group $F\bar{1}$). However, these two AO transitions differ from that of $(TMTSF)_2ClO_4$,[11-13] where the unit cell transforms from $a \times b \times c$, space group $P\bar{1}$, to $a \times 2b \times c$, space group $P\bar{1}$ at 24 K. The $X^- = BF_4^-$ and ReO_4^- salts are insulating below their AO transition temperatures,[1,8] but $(TMTSF)_2ClO_4$ remains metallic to ~1.2 K,[1] below which temperature it becomes superconducting at ambient pressure.[9] Also, superconductivity in $(TMTSF)_2ClO_4$ occurs only when the crystal is cooled slowly through its 24 K AO transition.[14,19,21] However, no cooling rate effects have yet been reported for the AO transition of $(TMTSF)_2BF_4$. The MI transitions in $(TMTSF)_2BF_4$[25] and

[†] Argonne National Laboratory.
[‡] North Carolina State University.
[§] Current address: Laboratoire de Chimie des Solides, Universite de Nantes, 44072 Nantes Cedex, France.

(1) Bechgaard, K. *Mol. Cryst. Liq. Cryst.* **1982**, *79*, 1 and references therein.
(2) Thorup, N.; Rindorf, G.; Soling, H.; Bechgaard, K. *Acta Crystallogr., Sect. B: Struct. Crystallogr. Cryst. Chem.* **1981**, *B37*, 1236.
(3) Williams, J. M.; Beno, M. A.; Sullivan, J. C; Banovetz, L. M.; Braam. J. M.; Blackman, G. S.; Carlson, C. D.; Greer, D. L.; Loesing, D. M. *J. Am. Chem. Soc.* **1983**, *105*, 643.
(4) Williams, J. M.; Beno, M. A.; Sullivan, J. C.; Banovetz, L. M.; Braam, J. M.; Blackman, G. S.; Carlson, C. D.; Greer, D. L.; Loesing, D. M.; Carneiro, K. *Phys. Rev. B: Condens. Matter* **1983**, *28*, 2873.
(5) Wudl, F. *J. Am. Chem. Soc.* **1981**, *103*, 7065.
(6) Whangbo, M.-H.; Williams, J. M.; Beno, M. A.; Dorfman, J. R. *J. Am. Chem. Soc.* **1983**, *105*, 645.
(7) Whangbo, M.-H.; Walsh, W. M., Jr.; Haddon, R. C.; Wudl, F. *Solid State Commun.* **1982**, *43*, 637.
(8) Bechgaard, K.; Jacobsen, C. S.; Mortensen, K.; Pedersen, H. J.; Thorup, N. *Solid State Commun.* **1980**, *33*, 1119.
(9) (a) Bechgaard, K.; Carneiro, K.; Rasmussen, F. B.; Olsen, M.; Rindorf, G.; Jacobsen, C. S.; Pedersen, H. J.; Scott, J. C. *J. Am. Chem. Soc.* **1981**, *103*, 2440. (b) Braam, J. M.; Carlson, C. D.; Stephens, D. A.; Rehan, A. E.; Compton, S. J.; Williams, J. M. *Inorg. Synth.* **1986**, *24*, 30.
(10) Jérome, D.; Mazaud, A.; Ribault, M.; Bechgaard, K. *J. Phys. (Les Ulis, Fr.) Lett.* **1980**, *41*, L95.
(11) Pouget, J. P.; Moret, R.; Comes, R.; Bechgaard, K.; Fabre, J. M.; Giral, L. *Mol. Cryst. Liq. Cryst.* **1982**, *79*, 129.
(12) Pouget, J. P.; Shirane, G.; Bechgaard, K.; Fabre, J. M. *Phys. Rev. B: Condens. Matter* **1983**, *27*, 5203.
(13) Kagoshima, S.; Yasunaga, T.; Ishiguro, T.; Anzai, H.; Saito, G. *Solid State Commun.* **1983**, *46*, 867.
(14) Tomic, S.; Jérome, D.; Monod, P.; Bechgaard, K. *J. Phys. (Les Ulis, Fr.) Colloq. C3, Suppl. 6*, **1983**, *44*, C3-1083.
(15) Mortensen, K.; Tomkiewicz, Y.; Schultz, T. D.; Engler. E. M. *Phys. Rev. Lett.* **1981**, *46*, 1234.
(16) Andrieux, A.; Jérome, D.: Bechgaard, K. *J. Phys. (Les Ulis, Fr.) Lett.* **1981**, *42*, L87.
(17) Mott, N. F. *Metal-Insulator Transitions*; Barnes & Noble: New York, 1977.
(18) Brandow, B. H. *Adv. Phys.* **1977**, *26*, 651.
(19) Takahashi, T.; Jérome, D.; Bechgaard, K. *J. Phys. (Les Ulis, Fr.), Colloq. C3, Suppl. 6*, **1983**, *44*, C3-805.
(20) Tomic, S.; Jérome, D.; Bechgaard, K. *J. Phys. C: Solid State Physics* **1984**, *17*, L11.
(21) Tomic, S.; Jérome, D.; Bechgaard, K. *Mol. Cryst. Liq. Cryst.* **1985**, *119*, 241.
(22) Leung, P. C. W.; Schultz, A. J.; Wang, H. H.; Emge, T. J.; Ball, G. A.; Cox, D. D.; Williams, J. M. *Phys. Rev. B: Condens. Matter* **1984**, *30*, 1615.
(23) Rindorf, G.; Soling, H.; Thorup, N. *Acta Crystallogr. Sect. C: Cryst. Struct. Commun.* **1984**, *C40*, 1137.
(24) Moret, R.; Pouget, J. P.; Comes, R.; Bechgaard, K. *Phys. Rev. Lett.* **1982**, *49*, 1008.
(25) Parkin, S. S. P.; Creuzet, F.; Ribault, M.; Jérome, D.; Bechgaard, K.; Fabre, J. M. *Mol. Cryst. Liq. Cryst.* **1982**, *79*, 249.

0002-7863/86/1508-8215$01.50/0

$(TMTSF)_2ReO_4$[26] can be suppressed under hydrostatic pressure. Under an applied pressure of ~10 kbar, $(TMTSF)_2ReO_4$ becomes superconducting at ~1.3 K,[26] but $(TMTSF)_2BF_4$ never becomes superconducting, even though it remains metallic to very low temperatures under such pressure ($T \sim 1$ K).[25] Also, the MI transitions for $(TMTSF)_2X$ salts with larger, centrosymmetric anions $X^- = PF_6^-$, AsF_6^-, and TaF_6^- occur at lower temperatures (~10 K),[8,25] compared to those with the smaller tetrahedral anions $X^- = BF_4^-$ (~40 K) and ReO_4^- (~180 K).[1,8] On the basis of heat capacity, electrical resistivity, and ESR measurements, the MI transitions of the $(TMTSF)_2X$ salts with the above octahedral anions occur upon SDW formation and do not involve crystallographic transitions.[15,16,25] However, these MI transitions are in one way similar to that of $(TMTSF)_2ReO_4$ and $(TMTSF)_2BF_4$, namely, they are suppressed under applied pressure. In fact, under hydrostatic pressure of ~12 kbar, all of the above $(TMTSF)_2X$ salts with octahedral anions become superconducting at ~1 K. Thus, the larger unit cell volumes of these octahedral anion salts contain the required *donor–donor* interactions and band electronic structures that allow SDW states and the ensuing MI transition to form at low temperature. This contrasts the behavior of the tetrahedral anion salts, which have smaller unit cell volumes by comparison and for which *donor–donor* interactions and anion ordering appear to be more important for producing the MI transition. Thus, the *symmetry* of the anion as well as its size has important consequences for the physical properties of a particular $(TMTSF)_2X$ salt.

The previously reported correlation between the size of the anion and the donor–donor (Se···Se) network for $(TMTSF)_2X$ salts has demonstrated that the *size of the anion* has important consequences for the electronic properties of each $(TMTSF)_2X$ salt.[3,4] Thus, an accurate description of donor–anion interactions is extremely important for an understanding of the physical behavior of these salts as well as for the rational design of new synthetic metals. The success of these efforts relies on the fact that $(TMTSF)_2X$ salts with different X^- anions contain systematic variations in their intermolecular (Se···Se) interactions[27-29] and, as a consequence, in their band electronic structures.[6]

It is also expected that the AO transitions which $(TMTSF)_2X$ salts undergo depend largely upon donor–anion interactions, of which there are two important types: Se···X and $-CH_3$···X. So far, only the Se···X type are known precisely, since only X-ray diffraction data have been available.[2-5] To describe the interactions of methyl group H atoms with anions in $(TMTSF)_2X$ salts, it is necessary to determine precise H atom locations, such as those obtained only from neutron diffraction data. Since this method requires large single crystals, the number of neutron diffraction studies of $(TMTSF)_2X$ salts to date has been limited.[30-32] In the present work, we carried out single crystal neutron diffraction studies for $(TMTSF)_2BF_4$ at 20 K and determined the precise H atom positions of the TMTSF methyl groups. This study enabled us to describe the structural features of the anion ordering, which occurs at ~40 K, in terms of short H···F contacts between BF_4^- anions and the TMTSF molecules. The nature of the metal–insulator transition in $(TMTSF)_2BF_4$, which coincides with the anion ordering transition, was investigated by performing tight binding band calculations for the 125 and 20 K crystal structures of $(TMTSF)_2BF_4$.

Table I. Crystallographic Data and 20 K Neutron Data Collection Parameters for $(TMTSF)_2BF_4$

A. Cell Data at 20, 125, and 298 K

	20 K	125 K	298 K
space group	$F\bar{1}$	$P\bar{1}$	$P\bar{1}$
Z	8	1	1
a (Å)	14.127 (4)	7.123 (1)	7.253 (1)
b (Å)	15.208 (4)	7.637 (1)	7.649 (2)
c (Å)	26.198 (6)	13.131 (2)	13.230 (2)
α (°)	85.00 (2)	85.38 (1)	85.29 (1)
β (°)	88.21 (2)	87.67 (1)	87.13 (1)
γ (°)	69.37 (2)	69.54 (1)	70.37 (1)
V (Å^3)	5247 (5)	668.0 (4)	688.8 (4)
ρ_{calcd}	2.488	2.443	2.369
formula			$Se_8C_{20}H_{24}{\cdot}BF_4$
molecular wt			982.90

B. 20 K Neutron Data Collection Parameters

cryst dimensns along a^*, b^*, c^* (mm)	4.0, 0.8, 0.7	(1.7 mm^3 vol)
absorptn coeff (cm^{-1})	2.42	
transmissn factors	0.89–0.99	
cooling rates (deg min^{-1})	slow cooling	fast cooling
	0.1 (1)	6 (1)
tot. reflectns collctd	5767	3572
unique data (n, in refinement)	4721	3101
superlattice data (ratio of odd hkl to even hkl)	41%	27%
$R(F) = \Sigma\|\|F_o\| - \|F_c\|\|/\Sigma\|F_o\|$	0.056	0.050
$wR(F) = [\Sigma w(\|F_o\| - \|F_c\|)^2/\Sigma F_o^2]^{1/2}$	0.061	0.052
GOF = $[\Sigma w(\|F_o\| - \|F_c\|)^2/(n-m)]^{1/2}$, for n obsrvtns and m = 515 variable params	1.673	1.798

Synthesis

Single crystals of $(TMTSF)_2BF_4$ suitable for neutron diffraction studies were grown by use of electrocrystallization techniques.[9a,9b,33] The key factors to the growth of these large single crystals include purifying and drying solvents and chemicals to the highest possible degree, the preparation of the electrodes prior to electrocrystallization, and careful control of the electrocrystallization conditions. The common practice for electrode preparation is to clean the platinum electrodes with a strong acid (HCl/HNO_3), but this procedure imparts an oxidized surface upon which crystals form poorly. The best preparation procedures are as follows: the anode for crystal growth is connected to the negative lead of a 3-V battery, and the cathode is connected to a timer switch then to the positive lead. Electrodes are then immersed in a 1 M H_2SO_4 solution. A potential is applied for 4 min, and gases should be produced on both electrodes, after which the polarity is reversed for 4 min. Finally, the polarity is switched back to the original configuration for another 8 min. The electrodes are rinsed and soaked with distilled water and then absolute methanol for 10 min each. A heat-gun is used to dry the electrodes. A large H configuration cell containing 80 mg of TMTSF (4.0 mM, Strem, gradient sublimed) and 1.50 g of $N(n\text{-}Bu)_4BF_4$ (0.10 M) in 45 mL of 1,1,2-trichloroethane (Aldrich, reflux over P_2O_5 and run through an activated alumina column) is used for electrocrystallization. A small constant current of 2.0 μA/cm^2 is applied, and the crystal growth is carried out in a constant temperature environment (23.0 ± 0.2 °C). Large single crystals on the order of 1 × 1 × 10 mm^3 are harvested after 4 weeks of crystal growth under these conditions to give a yield of approximately 70%.

Neutron Diffraction Data Collection

A crystal having a volume of 1.7(1) mm^3 (maximum and minimum linear dimensions of about 4.0 mm and 0.7 mm, respectively) was glued to the end of a hollow-tip aluminum pin and mounted under He in an aluminum can. This single-crystal mount was placed in a Displex closed-cycle refrigerator on a four-circle diffractometer at the high flux beam reactor at Brookhaven National Laboratory. The wavelength, 1.1599 (1) Å, of the Ge (220) monochromatized neutron beam was calibrated by using a KBr crystal [a_0 = 6.6000 (1) Å at 298 K].[34] The sample temperature was first lowered at a rate of ~2 deg min^{-1} from 298

(26) Parkin, S. S. P.; Jérome, D.; Bechgaard, K. *Mol. Cryst. Liq. Cryst.* **1982**, *79*, 213.
(27) Williams, J. M.; Beno, M. A.; Wang, H. H.; Emge, T. J.; Copps, P. T.; Hall, L. N.; Carlson, K. D.; Crabtree, G. W. *Philos. Trans. R. Soc. London, A* **1985**, *A314*, 83.
(28) Williams, J. M.; Beno, M. A.; Wang, H. H.; Leung, P. C. W.; Emge, T. J.; Geiser, U.; Carlson, K. D. *Acc. Chem. Res.* **1985**, *18*, 261.
(29) Beno, M. A.; Blackman, G. S.; Leung, P. C. W.; Williams, J. M. *Solid State Commun.* **1983**, *48*, 261.
(30) Gallois, B.; Gaultier, J.; Hauw, D.; Chasseau, D.; Meresse, A.; Filhol, A.; Bechgaard, K. *Mol. Cryst. Liq. Cryst.* **1985**, *119*, 225.
(31) Gallois, B.; Chasseau, D.; Gaultier, J.; Hauw, C.; Filhol, A.; Bechgaard, K. *J. Phys. (Les Ulis, Fr.), Colloq. C3, Suppl. 6*, **1983**, *44*, 1043–1071.
(32) Emge, T. J.; Williams, J. M.; Leung, P. C. W.; Schultz, A. J.; Beno, M. A.; Wang, H. H. *Mol. Cryst. Liq. Cryst.* **1985**, *119*, 237.
(33) Lee, M. M.; Stokes, J. M.; Wiygul, F. M.; Kistenmacher, T. J.; Cowan, D. O.; Poehler, T. O.; Bloch, A. N.; Fuller, W. W.; Gubser, D. U. *Mol. Cryst. Liq. Cryst.* **1982**, *79*, 145.
(34) *Crystal Data Determinative Tables*, Donnay, J. D. H., Ondik, H. M., Eds.; 3rd ed.; U. S. Department of Commerce and Joint Committee on Powder Diffraction Standards: Washington, DC, 1973; Vol. 2, C164.

to 75 K, followed by a rate of 0.2 deg min^{-1} from 75 to 60 K, and finally by 0.10 (5) deg min^{-1} from 60 to 20 K. The last stage involved slow cooling the crystal through its anion ordering phase transition. The temperature of 20 K remained essentially constant throughout the experiment, having maximum deviations of about ±0.01 deg. The temperature readings of the cryostat were previously calibrated with reference to the magnetic phase transition temperature of 78.39 (1) K in FeF_2.[35] The unit cell parameters that are listed in Table I were obtained from a least-squares fit of the $\sin^2\theta$ values for 32 reflections (16 Friedel pairs) in the $\sin\theta/\lambda$ range 0.347–0.444 $Å^{-1}$. The unconventional F-centered unit cell was selected in order to directly compare the $2a \times 2b \times 2c$ superstructure of $(TMTSF)_2BF_4$ at 20 K to its primitive $a \times b \times c$ high temperature cell at 125 or 298 K (see Table I). The 20 K superstructure of $(TMTSF)_2BF_4$ is isostructural to that of $(TMTSF)_2ReO_4$ at 120 K,[23] in which the AO transition occurs at 180 K. Neutron intensity data for the F-centered allowed reflections were collected in the θ–2θ scan mode. The intensities of two monitor reflections, which were measured after every 100 reflections, showed no significant variation throughout the experiment. Systematic absences of the F-centered lattice were confirmed by examining all reflections in the complete primitive $+h\pm k\pm l$ hemisphere for $0° < 2\theta < 30°$.

The crystal used in the above experiment was later warmed to room temperature (at ~2 deg min^{-1}) and then cooled at a moderately fast rate to 20 K (~6 deg min^{-1} for $T < 50$ K). A second data set was collected for this "fast-cooled" crystal in a similar manner to the previously described set (see Table I). Extinction effects appeared to be less dominant in this second data set, and on the basis of several ω-scan profiles from both data sets, the initial warming and cooling of the crystal probably increased the mosaic spread of the crystal. The diffraction intensities after slow cooling this crystal that were most affected by extinction had terms of 1.31 or less multiplying F^2_{obsd}.

The intensity level of the outermost five steps on both ends of each scan (~12–20% of the total scan) was used to compute the background intensity of each reflection. The net intensities were corrected for Lorentz effects and for absorption, the latter correction employing an analytical method.[36] The relative number of observations for sublattice (even *hkl* values) and superlattice (odd *hkl* values) reflections are included in Table I.

Crystallographic Results

Initial coordinates for all non-hydrogen atoms of the two crystallographically independent TMTSF molecules and the ordered BF_4^- anion were obtained by transforming the atomic positions of $(TMTSF)_2BF_4$ derived from 125 K X-ray data, in order to obtain positions corresponding to its $2a \times 2b \times 2c$ unit cell at 20 K. After the first few cycles of difference Fourier refinement,[37] this superstructure model converged rapidly, and all H atoms were located. The least-squares refinement of the positional and anisotropic thermal parameters of all 57 atoms, the scale factor and type I isotropic extinction[38] factor (a total of 515 variables), proceeded immediately to convergence and yielded the final R values given in Table I. The quantity minimized in the refinement was $\Sigma[w(F_o^2 - F_c^2)]$, with weights $w = 1/\sigma(F_o^2)$ and variances $\sigma^2(F_o^2) = \sigma_c^2(F_o^2) + (0.02F_o^2)^2$ [$\sigma_c(F_o^2)$ from counting statistics]. The final difference-density maps for either data set contained residual peaks on the order of 3–4% of a C atom peak in the area of C and Se atoms. Neutron scattering lengths[39] (10^{-12} cm) that were used included the following: $b_H = -0.3741$, $b_C = 0.6648$, $b_F = 0.565$, $b_{Se} = 0.797$. The refined b_B was 0.558 (5) $\times 10^{-12}$ cm which was very close to the value for naturally occurring boron (0.535×10^{-12} cm). Thus, the scattering length of the one B atom was fixed to 0.535×10^{-12} cm for the final cycles of refinement. The final atomic coordinates and equivalent isotropic thermal parameters of the two independent TMTSF molecules and the ordered BF_4^- anion are given in Table II for both slow- and fast-cooling experiments. Since the final values of the atomic parameters for the fast-cooling data set are not significantly different from those for the slow-cooling data set, only the crystallographic results for the slow-cooled crystals will be used for the discussion below. The bond distances and angles for the BF_4^- anion and the two independent TMTSF molecules are given in Table III.

Table II. Positional and Equivalent (U_{equiv}) Thermal Parameters for $(TMTSF)_2BF_4$ at 20 K after Slow Cooling[a]

atom	x	y	z	U_{equiv}
Se11	4042 (2)	1702 (1)	3098 (1)	39 (16)
Se12	3302 (1)	3770 (2)	2565 (1)	33 (16)
Se13	3617 (1)	2906 (1)	1396 (1)	28 (16)
Se14	4387 (2)	829 (2)	1927 (1)	32 (17)
C11	3768 (2)	2473 (2)	2482 (1)	43 (19)
C12	3656 (1)	2725 (1)	3519 (1)	54 (21)
C13	3337 (2)	3606 (2)	3290 (1)	49 (20)
C14	3737 (1)	2444 (1)	4085 (1)	56 (22)
C15	2979 (2)	4511 (2)	3548 (1)	57 (22)
C16	3903 (1)	2124 (2)	2009 (1)	37 (20)
C17	4038 (1)	1889 (1)	977 (1)	43 (19)
C18	4369 (2)	995 (1)	1204 (1)	54 (20)
C19	3976 (2)	2130 (2)	405 (1)	65 (22)
C10	4732 (2)	118 (2)	921 (1)	56 (21)
H14A	3298 (5)	1999 (5)	4194 (2)	26 (6)
H14B	4520 (4)	2037 (4)	4190 (2)	25 (5)
H14C	3488 (6)	3063 (4)	4304 (2)	27 (6)
H15A	3150 (4)	4397 (4)	3955 (2)	26 (6)
H15B	3342 (4)	4994 (4)	3378 (3)	27 (6)
H15C	2168 (4)	4855 (4)	3501 (2)	25 (6)
H19A	3454 (4)	1861 (5)	240 (2)	27 (6)
H19B	3724 (5)	2883 (4)	308 (2)	31 (5)
H19C	4710 (4)	1801 (4)	227 (3)	32 (5)
H10A	4488 (5)	−429 (3)	1105 (3)	34 (6)
H10B	5545 (4)	−157 (4)	898 (3)	30 (6)
H10C	4437 (5)	262 (4)	534 (2)	27 (6)
Se21	4017 (1)	6701 (1)	3081 (1)	34 (16)
Se22	3274 (1)	8781 (1)	2556 (1)	39 (16)
Se23	3577 (1)	7922 (1)	1379 (1)	32 (16)
Se24	4380 (1)	5838 (1)	1903 (1)	31 (16)
C21	3750 (2)	7481 (2)	2465 (1)	48 (21)
C22	3633 (2)	7723 (2)	3509 (1)	46 (20)
C23	3317 (2)	8608 (1)	3285 (1)	45 (21)
C24	3716 (1)	7434 (1)	4073 (1)	68 (22)
C25	2968 (2)	9506 (1)	3544 (1)	59 (22)
C26	3885 (1)	7141 (2)	1995 (1)	48 (20)
C27	3984 (2)	6908 (1)	956 (1)	55 (20)
C28	4341 (2)	6020 (1)	1178 (1)	51 (20)
C29	3898 (2)	7164 (1)	386 (1)	73 (22)
C20	4724 (2)	5145 (2)	892 (1)	61 (22)
H24A	3299 (5)	6958 (4)	4175 (2)	25 (6)
H24B	4501 (4)	7054 (5)	4181 (2)	26 (6)
H24C	3408 (4)	8043 (4)	4296 (2)	26 (5)
H25A	3076 (4)	9384 (4)	3959 (2)	26 (6)
H25B	3370 (5)	9960 (4)	3391 (2)	25 (6)
H25C	2166 (4)	9882 (4)	3468 (2)	22 (6)
H29A	3496 (5)	6787 (5)	205 (3)	28 (6)
H29B	3518 (6)	7910 (4)	299 (2)	41 (6)
H29C	4646 (4)	6968 (5)	215 (2)	42 (6)
H20A	4467 (4)	4595 (4)	1076 (2)	30 (6)
H20B	5548 (4)	4878 (5)	878 (2)	28 (6)
H20C	4445 (5)	5286 (4)	502 (2)	28 (6)
B	2534 (2)	37 (2)	−33 (1)	49 (16)
F1	3485 (1)	−579 (1)	−177 (1)	105 (17)
F2	2656 (1)	714 (2)	265 (1)	75 (18)
F3	2020 (2)	−478 (1)	247 (1)	147 (19)
F4	1975 (2)	501 (2)	−470 (1)	105 (19)

[a] Fractional coordinates are $\times 10^4$, U_{equiv} values are $\times 10^4$ for non-hydrogen atoms and $\times 10^3$ for H atoms, where $U_{equiv} = 1/(6\pi^2)\Sigma\beta_{ij}a_ia_j$. Estimated standard deviations are enclosed in parentheses.

Discussion

Crystallographic Ordering of the BF_4^- Anions. At 20 K, there are very small and nearly isotropic thermal parameters for the B and F atoms of the anion (see Table II), whose geometry is tetrahedral within experimental errors (i.e., average B–F distances of 1.400 (1) Å and F–B–F angle of 109.5 (2)°, from Table III). Thus, with the use of the superstructure neutron data, the molecular structure of the BF_4^- anion is found to be *completely ordered* at 20 K. It is now of interest to examine the relative

(35) Hutchings, M. T.; Schulhof, M. P.; Guggenheim, H. J. *Phys. Rev. B: Solid State* **1972**, *5*, 154.
(36) Coppens, P.; Leiserowitz, L. L.; Rabinovich, D. *Acta Crystallogr.* **1965**, *18*, 1035.
(37) McMullan, R. K., unpublished results.
(38) Becker, P. J.; Coppens, P. *Acta Crystallogr., Sect. A: Cryst. Phys., Diffr., Theo. Gen. Crystallogr.* **1975**, *A31*, 417.
(39) Koester, L.; Rauch, H.; Herkens, M.; Schröder, K. Report Jül-1755, Kernforschungsanlage Jülich, 1981.

Table III. Bond Distances (Å) and Angles (deg) for $(TMTSF)_2BF_4$ at 20 K[a]

A. The TMTSF Molecular Geometries

molecule A		molecule B		molecule A		molecule B	
Se11-C11	1.878 (2)	Se21-C21	1.882 (2)	C18-C10	1.501 (3)	C28-C20	1.504 (3)
Se11-C12	1.896 (3)	Se21-C22	1.907 (3)	C14-H14A	1.083 (5)	C24-H24A	1.093 (5)
Se12-C11	1.877 (3)	Se22-C21	1.885 (3)	C14-H14B	1.092 (5)	C24-H24B	1.088 (5)
Se12-C13	1.894 (3)	Se22-C23	1.905 (3)	C14-H14C	1.091 (5)	C24-H24C	1.088 (5)
Se13-C16	1.878 (2)	Se23-C26	1.884 (2)	C15-H15A	1.086 (5)	C25-H25A	1.094 (5)
Se13-C17	1.886 (2)	Se23-C27	1.889 (3)	C15-H15B	1.093 (5)	C25-H25B	1.083 (5)
Se14-C16	1.873 (2)	Se24-C26	1.889 (3)	C15-H15C	1.084 (5)	C25-H25C	1.091 (5)
Se14-C18	1.889 (2)	Se24-C28	1.896 (2)	C19-H19A	1.078 (5)	C29-H29A	1.080 (5)
C11-C16	1.370 (3)	C21-C26	1.360 (3)	C19-H19B	1.082 (5)	C29-H29B	1.078 (5)
C12-C13	1.346 (3)	C22-C23	1.345 (3)	C19-H19C	1.088 (5)	C29-H29C	1.085 (5)
C12-C14	1.501 (3)	C22-C24	1.501 (3)	C10-H10A	1.081 (5)	C20-H20A	1.094 (5)
C13-C15	1.502 (3)	C23-C25	1.494 (3)	C10-H10B	1.076 (5)	C20-H20B	1.090 (5)
C17-C18	1.359 (3)	C27-C28	1.348 (3)	C10-H10C	1.084 (5)	C20-H20C	1.084 (5)
C17-C19	1.511 (3)	C27-C29	1.508 (3)				

molecule A		molecule B		molecule A		molecule B	
C11-Se11-C12	94.5 (1)	C21-Se21-C22	94.5 (1)	H14A-C14-H14C	109.9 (5)	H24A-C24-H24C	108.0 (4)
C11-Se12-C13	94.3 (1)	C21-Se-22-C23	94.5 (1)	H14B-C14-H14C	107.6 (4)	H24B-C24-H24C	109.3 (4)
C16-Se13-C17	93.9 (1)	C26-Se23-C27	94.3 (1)	H14A-C14-C12	111.0 (3)	H24A-C24-C22	110.7 (3)
C16-Se14-C18	94.1 (1)	C26-Se24-C28	94.1 (1)	H14B-C14-C12	110.4 (3)	H24B-C24-C22	110.5 (3)
Se11-C11-Se12	114.3 (1)	Se21-C21-Se22	114.1 (1)	H14C-C14-C12	110.9 (3)	H24C-C24-C22	111.2 (3)
C16-C11-Se11	123.2 (2)	C26-C21-Se21	123.2 (2)	H15A-C15-H15B	107.5 (4)	H25A-C25-H25B	109.1 (4)
C16-C11-Se12	122.6 (2)	C26-C21-Se22	122.7 (2)	H15A-C15-H15C	108.4 (4)	H25A-C25-H25C	108.1 (4)
C13-C12-Se11	118.2 (2)	C23-C22-Se21	118.5 (2)	H15C-C15-H15B	107.9 (4)	H25B-C25-H25C	107.3 (4)
C14-C12-Se11	114.7 (2)	C24-C22-Se21	114.6 (2)	H15A-C15-C13	112.0 (3)	H25A-C25-C23	112.3 (3)
C13-C12-C14	127.1 (2)	C23-C22-C24	126.9 (2)	H15B-C15-C13	110.6 (3)	H25B-C25-C23	110.1 (3)
C12-C13-Se12	118.8 (2)	C22-C23-Se22	118.5 (2)	H15C-C15-C13	110.2 (3)	H25C-C25-C23	109.7 (3)
C15-C13-Se12	114.2 (2)	C25-C23-Se22	114.1 (2)	H19A-C19-H19B	108.3 (4)	H29A-C29-H29B	109.0 (5)
C12-C13-C15	127.1 (2)	C22-C23-C25	127.4 (2)	H19A-C19-H19C	107.2 (4)	H29A-C29-H29C	107.0 (5)
Se14-C16-Se13	114.9 (1)	Se23-C26-Se24	114.1 (1)	H19B-C19-H19C	109.0 (4)	H29B-C29-H29C	108.0 (5)
C11-C16-Se13	122.6 (2)	C21-C26-Se23	123.2 (2)	H19A-C19-C17	109.9 (3)	H29A-C29-C27	111.1 (3)
C11-C16-Se14	122.4 (2)	C21-C26-Se24	122.7 (2)	H19B-C19-C17	111.9 (3)	H29B-C29-C27	111.5 (3)
C18-C17-Se13	118.8 (2)	C28-C27-Se23	118.8 (2)	H19C-C19-C17	110.5 (3)	H29C-C29-C27	110.0 (3)
C19-C17-Se13	117.0 (1)	C29-C27-Se23	116.4 (2)	H10A-C10-H10B	107.8 (5)	H20A-C20-H20B	109.0 (5)
C18-C17-C19	124.2 (2)	C28-C27-C29	124.7 (2)	H10A-C10-H10C	107.0 (5)	H20A-C20-H20C	107.1 (4)
C17-C18-Se14	118.2 (2)	C27-C28-Se24	118.6 (2)	H10B-C10-H10C	107.9 (5)	H20B-C20-H20C	108.0 (5)
C10-C18-Se14	116.9 (1)	C20-C28-Se24	116.6 (1)	H10A-C10-C18	111.8 (3)	H20A-C20-C28	110.7 (3)
C17-C18-C10	124.8 (2)	C27-C28-C20	124.9 (2)	H10B-C10-C18	111.2 (3)	H20B-C20-C28	110.6 (3)
H14A-C14-H14B	106.9 (4)	H24A-C24-H24B	107.1 (4)	H10C-C10-C18	110.8 (3)	H20C-C20-C28	111.2 (3)

B. The BF_4^- Anion Geometry

molecule A		molecule B		molecule A		molecule B	
B-F1	1.403 (3)	B-F3	1.398 (3)	F1-B-F2	109.8 (4)	F2-B-F3	109.9 (4)
B-F2	1.406 (3)	B-F4	1.398 (3)	F1-B-F3	109.2 (4)	F2-B-F4	108.6 (4)
				F1-B-F4	109.7 (4)	F3-B-F4	109.6 (4)

[a] Estimated standard deviations are enclosed in parentheses.

distances between the BF_4^- anion and neighboring TMTSF molecules, especially any short donor–anion contacts which may be the result of electron localization.

Listed in Table IVA are the relative center-of-mass displacements between the BF_4^- anion and the ten nearest-neighbor TMTSF molecules. The four TMTSF molecules that are nearest the BF_4^- anion, which are labeled A1, A2, A5, and B5 in Figure 1, contain the eight shortest H···F contacts (see Table IVB). The BF_4^- anion is displaced approximately 0.12 Å from the pseudo-symmetry center (i.e., from the point $x = {}^1/_4$, $y = 0$, $z = 0$ of the $2a \times 2b \times 2c$ F-centered supercell at 20 K). Above the AO transition, the anion is, within experimental error, centered directly on the $({}^1/_2, 0, 0)$ inversion center of the $a \times b \times c$ primitive cell. The donor–anion separations are described in Table IVA by D_{ij} values, which are distances between the TMTSF molecule (i) and BF_4^- anion (j): $D_{ij} = (\Delta X_{ij}^2 + \Delta Y_{ij}^2 + \Delta Z_{ij}^2)^{1/2}$, where (X_i,Y_i,Z_i) and (X_j,Y_j,Z_j) are local Cartesian coordinates of the TMTSF and BF_4^- species, respectively. As indicated by the D_{ij} values in Table IVA, the high temperature (298 and 125 K) separations between the BF_4^- anion and TMTSF molecule A are identical by symmetry to those between the BF_4^- anion and TMTSF molecule B. At 20 K, the D_{ij} distance between one anion and TMTSF molecule A differs markedly from that between the same anion and TMTSF molecule B (see Table IVA). The approximate direction of the BF_4^- anion displacement from the pseudo-symmetry center $({}^1/_4, 0, 0)$ at 20 K is toward TMTSF molecules A1 and A5 and away from molecule B5 (see Figure 1). On the basis of the D_{ij} values in Table IVB, the distances from the BF_4^- anion to all nearby TMTSF molecules contract by similar amounts as the temperature is lowered from 298 to 125 K [the average of the decreases in D_{ij} values is ~0.05 (2) Å]. However, upon further cooling from 125 to 20 K, the D_{ij} distances change anisotropically, since those to TMTSF molecules A1 and B4 greatly *decrease* (by 0.15 and 0.14 Å, respectively) and those to molecules B3 and B5 noticeably *increase* (by 0.08 Å and 0.07 Å, respectively). Also, one Se···F contact at 20 K, which is shorter than the van der Waals radii[40] sum of 3.35 Å (vide infra), exists between the BF_4^- anion and TMTSF molecule A1, but no short Se···F distances are observed between the anion and TMTSF molecules of type B. Thus, it is possible that Coulombic attraction between the BF_4^- anion and

(40) (a) Pauling, L. *The Nature of the Chemical Bond*, 3rd ed.; Cornell University Press: Ithaca, New York, 1960; p 260. (b) Bondi, A. *J. Phys. Chem.* **1964**, *68*, 441.

Table IV. Interaction Distances between TMTSF Molecules and BF_4^- Anions in $(TMTSF)_2BF_4$ at 20, 125, and 298 K

A. Distances between Centroids of TMTSF Donor (i) and BF_4^- Anion (j) at 20/125/298 K[a]

TMTSF	D_{ij} (Å)	D_1	D_2	TMTSF	D_{ij} (Å)	D_1	D_2
A1[b]	6.69/6.84/6.90	0.15	0.06	B1	6.84/6.84/6.90	0.00	0.06
A2	7.72/7.72/7.77	0.00	0.05	B2	7.65/7.72/7.77	0.07	0.05
A3	7.83/7.89/7.97	0.06	0.08	B3	7.97/7.89/7.97	-0.08	0.08
A4	8.32/8.26/8.27	-0.06	0.01	B4	8.12/8.26/8.27	0.14	0.01
A5	8.40/8.46/8.51	0.06	0.05	B5	8.53/8.46/8.51	-0.07	0.05

B. C-H···F Interaction Distances and Angles

F···H contact	distances 20K	angles 20 K	contact	F···C distances 20 K	125 K	298 K
F2···H25A	2.269 (5)[c]	146.6 (2)	F2···C25	3.239 (3)	3.34 (1)	3.39 (2)
F2···H24C	2.329 (5)	164.6 (2)	F2···C24	3.391 (3)	3.46 (1)	3.47 (2)
F1···H15A	2.339 (5)	170.4 (2)	F1···C15	3.415 (3)	3.50 (2)	3.60 (2)
F4···H19B	2.375 (5)	155.7 (2)	F4···C19	3.391 (3)	3.51 (2)	3.42 (2)
F2···H19A	2.383 (5)	149.4 (2)	F2···C19	3.355 (3)	3.38 (1)	3.52 (3)
F2···H10C	2.472 (6)	127.6 (2)	F2···C10	3.249 (3)	3.34 (1)	3.49 (3)
F4···H15A	2.480 (6)	117.5 (2)	F4···C15	3.134 (3)	3.14 (1)	3.13 (2)
F1···H29B	2.503 (5)	149.2 (2)	F1···C29	3.473 (3)	3.52 (2)	3.56 (2)

C. Donor-Anion Se···F Distances

contact	20 K	125 K	298 K
F4···Se13	3.180 (3)	3.30 (2)	3.22 (2)
F3···Se23	3.862 (3)	3.84 (2)	4.13 (4)[d]

[a] The displacements of TMTSF molecule i with respect respect to BF_4^- anion j is $D_{ij} = (\Delta X^2 + \Delta Y^2 + \Delta Z^2)^{1/2}$, where the local Cartesian coordinates (X_i, Y_i, Z_i) refer to the TMTSF centroid (the midpoint of the central C=C bond) and (X_j, Y_j, Z_j) refer to the BF_4^- centroid (the B atom). The differences $[D_{ij}$ (125 K) - D_{ij} (20 K)] and $[D_{ij}$ (298 K) - D_{ij} (125 K)] are D_1 and D_2, respectively. [b] Symmetry operations for the TMTSF molecules used here are molecules of type A: A1, $^1/_2 - x, ^1/_2 - y, -z$; A2, x, y, z; A3, $1 - x, -y, -z$; A4, $^1/_2 - x, -y, ^1/_2 - z$; A5, $x, -^1/_2 + y, -^1/_2 + z$, and molecules of type B: B1, $x, -1 + y, z$; B2, $^1/_2 - x, ^1/_2 - y, -z$; B3, $-^1/_2 + x, -^1/_2 + y, z$; B4, $x, -^1/_2 + y, -^1/_2 + z$; B5, $^1/_2 - x, 1 - y, ^1/_2 - z$. [c] Estimated standard deviations are enclosed in parentheses. [d] The F3 atom has extremely large thermal motion or positional disorder at 298 K (see text).

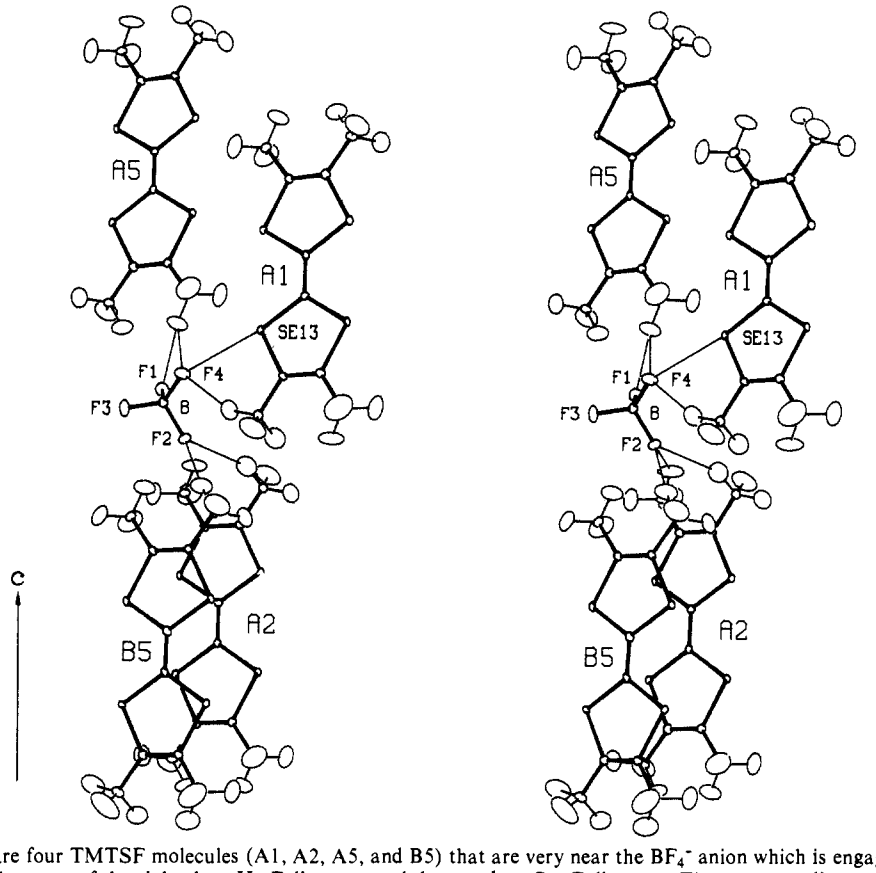

Figure 1. At 20 K, there are four TMTSF molecules (A1, A2, A5, and B5) that are very near the BF_4^- anion which is engaged in many donor-anion contacts (thin lines), namely, seven of the eight short H···F distances and the one short Se···F distance. These contact distances are short in comparison to the associated van der Waals radii[40] sums of 2.55 and 3.35 Å, respectively (see Table IV). The above stereoview is along the crystallographic *a* axis and contains thermal ellipsoids drawn at the 75% probability level.[48]

molecules A1 and B4 dominates the donor-anion interactions of $(TMTSF)_2BF_4$ below T_{AO}. In general, of the two different types of TMTSF molecules at 20 K (A and B), one is much closer to the nearest BF_4^- anion, whereas at temperatures above the anion ordering temperature, these donor-anion separations are equivalent.

Donor-Anion Contacts. The displacement of the BF_4^- anion toward TMTSF molecule A1 as the temperature is lowered also

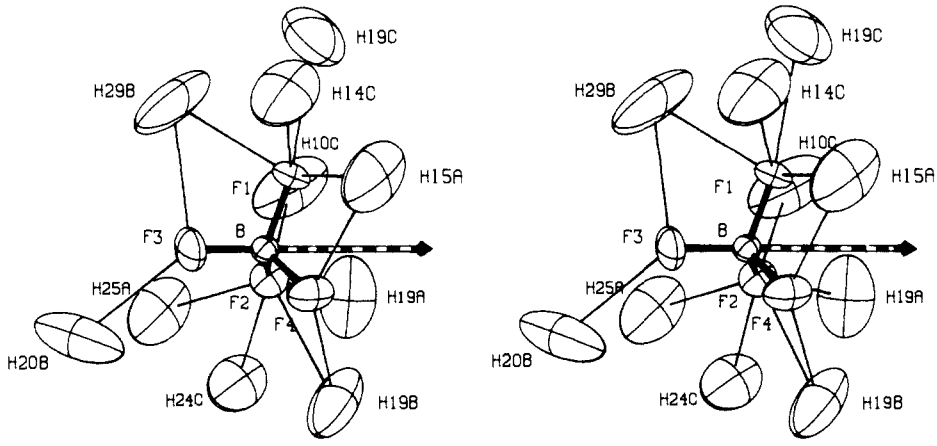

Figure 2. A stereoview of the H atom environment that surrounds the BF_4^- anion of $(TMTSF)_2BF_4$ at 20 K. The arrow indicates the direction of the relative displacement of the anion at 20 K with respect to its position at 125 K. Thermal ellipsoids are drawn at the 99% probability level.[48]

results in the shortening of the Se13···F4 contact 3.30 Å at 125 K to 3.18 Å at 20 K (see Table IVC), where it is 0.17 Å shorter than the van der Waals radii[40] (VDW) sum. The shortest Se···F distance to the other TMTSF molecule (B1) at 20 K is Se23···F3 at 3.863 (2) Å, but this distance is about 0.5 Å longer than the associated VDW sum (see Table IVC). For comparison, the very short Se···O contact in the ($2a \times 2b \times 2c$) superstructure of $(TMTSF)_2ReO_4$ is 2.991 (7) Å at 120 K.[23] Unfortunately, a comparison of the packing arrangement between cations and anions in these two salts by means of the H···X contacts is not possible, since the H atom positions in $(TMTSF)_2ReO_4$ are not accurately known.

For the complete description of donor–anion interactions in $(TMTSF)_2BF_4$, we now consider the eight H···F contacts between the BF_4^- anion and TMTSF molecules which are less than the VDW for H-F of 2.55 Å. The associated H···F distances and C-H···F angles for these contacts are listed in Table IVB and have ranges of 2.27–2.50 Å and 118–170°, respectively. The geometries of these contacts (i.e., short and having angles approaching 180°) are consistent with rather ionic crystal packing interactions involving H atoms.[41-43] The C-H distances and H-C-H angles for all methyl groups that are included in Table III, which average 1.086 (1) Å and 108.0 (2)°, respectively, demonstrate that no significant deviations from sp^3 geometry for any methyl C atoms due to H bonding or other effects are present at 20 K.

The H atom positions in $(TMTSF)_2BF_4$ at temperatures above its AO transition temperature are not accurately known, and a detailed comparison of H···F contacts above and below the 40-K phase transition is not possible. However, the relative direction of the BF_4^- anion displacement upon lowering the temperature can be illustrated by examining the relative positions of the C atoms at 125 and 20 K. The shortest C···F distances in $(TMTSF)_2BF_4$ at 298, 125, and 20 K are included in Table IVB. As depicted in Figure 2, the anion cavity at 20 K is characterized by an enclosure of H atoms. The relative BF_4^- anion displacement on going from 125 to 20 K is approximately away from F3 along a threefold axis. Thus, we expect that H···F contacts with atoms F1, F2, and F4 would have contracted more than those with F3 upon cooling the $(TMTSF)_2BF_4$ crystal through the AO transition. It is noted from Table IVB that among the H···F contacts less than or equal to the VDW sum, 2.55 Å, there are *none with F3*. It is noted that at all temperatures measured, F3 has much larger mean-squared displacements than the other F atoms (see the U_{equiv} values of the F atoms in Table II). Thus, the significant packing interactions between the BF_4^- anion and nearby TMTSF molecules, as evidenced by short cation–anion contacts and small thermal motion, involve *only* F1, F2, and F4. As a result, the

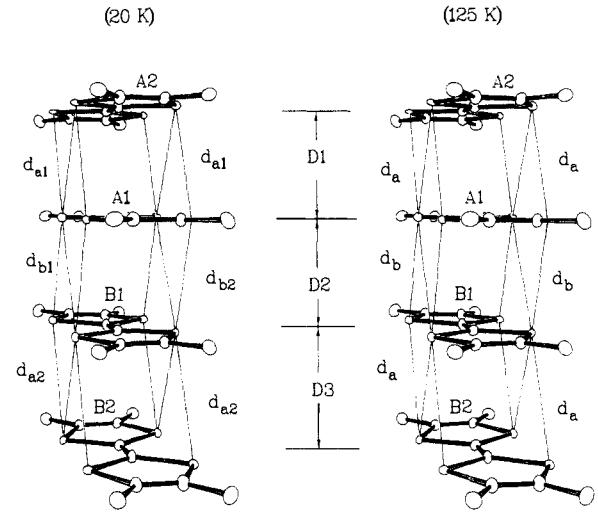

Figure 3. The two adjacent pairs of TMTSF molecules in a stack, A1–A2 and B1–B2, are different at 20 K (left), but are equivalent at 125 K (right), as noted from the values for the average Se···Se contact distances d_{a1}, d_{a2}, d_{b1}, and d_{b2} that are given in Table VC.

interactions that involve these three F atoms are likely to be the most important ones for anion-ordering in $(TMTSF)_2BF_4$.

Dimerization of the TMTSF Network. Dimerization of the crystallographic lattice occurs in $(TMTSF)_2BF_4$ at about 40 K,[22] which results in a metal–insulator transition.[1] The degree of dimerization in the low-temperature phase (at 20 K) vs. that in the high-temperature phase (at 125 or 298 K) is measured by (i) a comparison of the interplanar separations between TMTSF molecules and (ii) the variations of intra- and interstack Se···Se contact distances, both of which are given in Table V. The two unique dimeric units of TMTSF molecules that are illustrated in Figure 3 are A1–A2 and B1–B2. At 20 K, one intradimer separation, A1–A2, is 0.06 Å narrower than that of the other, B1–B2. At temperatures above the AO transition, the dimer pairs A1–A2 and B1–B2 are equivalent and coparallel, so that all donor–donor dihedral angles are zero. As the temperature is decreased from 125 to 20 K, however, the A1–A2 intradimer separation contracts by 0.05 Å and the separation between dimers (A1···B1) have an associated 0.4° dihedral angle between TMTSF molecule planes. As described in the previous section, the sole close Se···F contact and the majority of close H···F contacts involve TMTSF molecule A of the A1–A2 dimer.

There are important Se···Se distances that are less than or equal to the VDW sum of 4.0 Å. The short Se···Se contacts within a donor stack are listed as d1–d6 in Table VB, and these contacts are indicated by thin lines in Figure 3. The shortest Se···Se contacts between TMTSF molecules in adjoining stacks are listed as d7–d10 in Table VB. The variations of intrastack (d1–d6) and interstack (d7–d10) contacts vs. temperature are plotted in Figure

(41) Hamilton, W. C.; Ibers, J. A. *Hydrogen Bonding in Solids*; W. A. Benjamin: New York, New York, 1968; pp 14–21.
(42) Taylor, R.; Kennard, O. *Acc. Chem. Res.* **1984**, *17*, 320.
(43) Berkovitch-Yellin, Z.; Leiserowitz, L. *Acta Crystallogr., Sect. B: Struct. Sci.* **1984**, *B40*, 159.

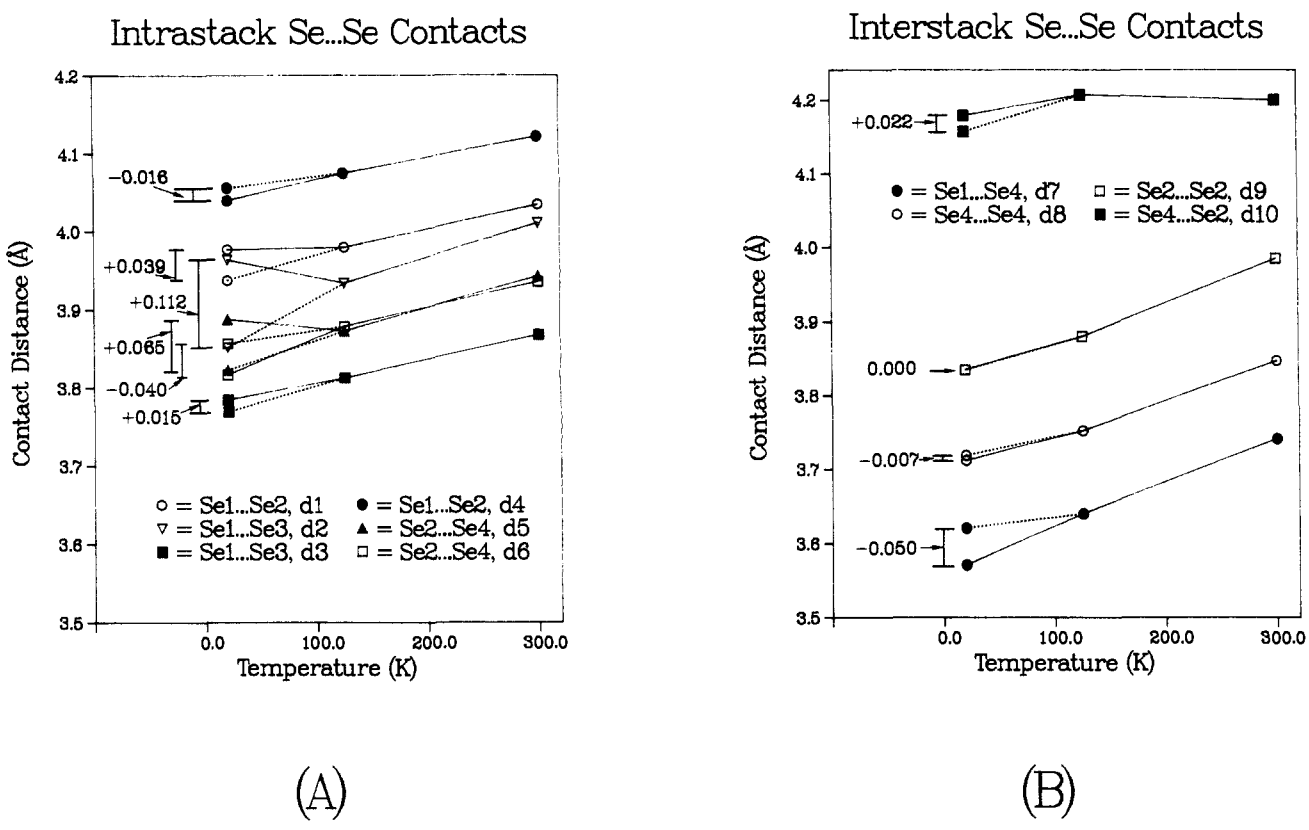

Figure 4. Variation of the shortest intrastack (A) and shortest interstack (B) Se···Se contact distances vs. temperature. The differences (see arrows) in the two 20 K values for each Se···Se distance *within* a stack are greater than those *between* stacks, so that the major distortions from anion ordering to the TMTSF molecule network are those involving the *stacking* of TMTSF molecules (see text).

4. As a result of the lattice dimerization which accompanies the AO transition, there are *two corresponding values* for Se···Se contacts d1–d7 and d9–d10, compared to one value at high temperature (see Table VB). Since contact d8 spans an inversion site at 20 K, it has a unique value. Given in Table VC are the *average* Se···Se contact distances between two adjacent TMTSF molecules within a given stack. At temperatures above the phase transition, these values are defined as the following: $d_a = (d_1 + d_2 + d_5)/3$ and $d_b = (d_3 + d_4 + d_6)/3$, with respect to the d1–d6 values from Table VB. Since there is a dimerized lattice at 20 K, these average contact distances also have two components each, namely, d_{a1}, d_{a2}, d_{b1}, and d_{b2}, with values listed in Table VC. At 20 K, d_{a2} is 0.07 Å *longer* than the other three mean distances, primarily because of the 0.4° dihedral angle between TMTSF molecules A1 and B1 at that temperature. All Se···Se contact distances at 20 K are shorter than their corresponding distances at 125 K, *except* contacts d2 and d5 between TMTSF molecules B1–B2 (see Table VB). Since both d2 and d5 contribute to the mean distance d_{a2} at 20 K, there is a 0.07 Å difference (i.e., $d_{a2} - d_{a1}$) in the average *intrastack* Se···Se distance between TMTSF molecules A1–A2 compared to that between molecules B1–B2. This difference is large compared to that between mean *interstack* Se···Se distances (i.e., $d_{b2} - d_{b1} = 0.01$ Å). Thus, along the *a* axis, the high conductivity axis,[1] the largest changes in donor–donor contacts upon the dimerization of the lattice exist. The consequences of the new donor–donor packing motif in $(TMTSF)_2BF_4$ at 20 K as a result of this dimerization for its band electronic structure are examined next.

Consequences of Lattice Dimerization for the Band Electronic Structure. A $(TMTSF)_2X$ salt having two TMTSF molecules per unit cell leads to two HOMO bands (i.e., those bands derived largely from the HOMO's of TMTSF molecules).[6,7] It is the higher lying band of the two that becomes partially filled and is, therefore, responsible for the metallic properties of the $(TMTSF)_2X$ salt. In the present section, we will investigate how the AO transition at 40 K affects the band electronic structure of $(TMTSF)_2BF_4$ and whether or not the BF_4^- anion orbitals participate at all in the valence band (i.e., the highest occupied band) of $(TMTSF)_2BF_4$. Thus, we performed tight binding band calculations for the crystal structures of $(TMTSF)_2BF_4$ determined at 125 and 20 K, in which all the atoms of a unit cell were included and double-ζ Slater-type orbitals were employed for B, C, F, and Se.[44]

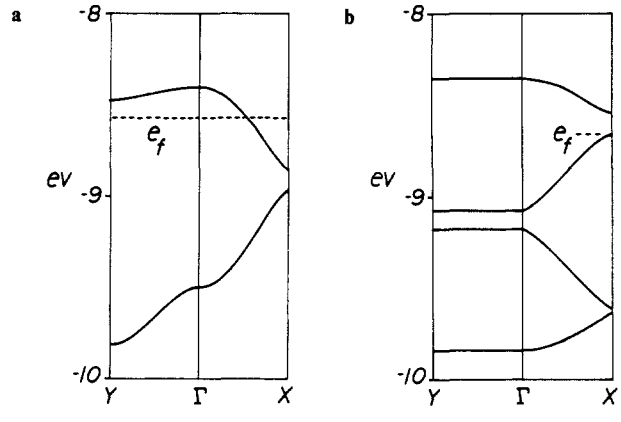

Figure 5. (a) Dispersion of the two HOMO bands of $(TMTSF)_2BF_4$ at 125 K along the wavevector directions $\Gamma \rightarrow X$ and $\Gamma \rightarrow Y$, where $\Gamma = (0,0)$, $X = (a^*/2, 0)$, and $Y = (0, b^*/2)$, and the dashed line is the Fermi level. (b) Dispersion of the four HOMO bands of $(TMTSF)_2BF_4$ at 20 K along the wavevector directions $\Gamma \rightarrow X$ and $\Gamma \rightarrow Y$. $\Gamma = (0,0)$, $X = (a'^*/2, 0)$, and $Y = (0, b'^*/2)$, where the reciprocal lattice constants a'^* and b'^* of the 20 K structure are related to those (a^* and b^*) of the 125 K structure as follows: $a'^* = a^*/2$, and $b'^* = b^*/2$.

(44) For boron, carbon, fluorine, and selenium, each atomic orbital was represented by a linear combination of two Slater-type orbitals of exponents ζ_μ and ζ_μ' with the weighting coefficients c_μ, and c_μ', respectively.[45] The ζ_μ, ζ_μ', c_μ, c_μ' and $H_{\mu\mu}$ (valence-shell ionization potential) values employed in our study are respectively 1.413, 0.876, 0.8409, 0.1788, and −15.2 eV for B 2s; 2.217, 1.006, 0.2153, 0.8404, and −8.50 eV for B 2p; 1.831, 1.153, 0.7616, 0.2630 and −21.4 eV for C 2s; 2.730, 1.257, 0.2595, 0.8025, and −11.4 eV for C 2p; 3.139, 1.900, 0.5822, 0.4846, and −20.5 eV for Se 4s; and 2.715, 1.511, 0.5347, 0.5553, and −14.4 eV for Se 4p. A modified Wolfsberg–Helmholz formula[46] was used to calculate $H_{\mu\nu}$.

Table V. Interaction Distances between TMTSF Molecules in $(TMTSF)_2BF_4$ at 20, 125, and 298 K

A. Interplanar Distances for the TMTSF Molecules Along the Stacking Axis

label[a]	between TMTSF molecules	separation (Å) 20/125/298 K
D1[b]	A1–A2	3.50/3.55/3.63
D2	A1···B1	~3.54[c]/3.57/3.62
D3	B1–B2	3.56/3.55/3.63

B. Se···Se Contact Distances between TMTSF Molecules

label[a]	20 K superstructure from molecule A1		from molecule B1		high-temperature phase 125 K	298 K
			1. Intrastack			
d1	Se11···Se12	3.941[d]	Se21···Se22	3.976	3.981	4.035
d2	Se11···Se13	3.853	Se21···Se23	3.963	3.933	4.011
d3	Se11···Se23	3.771	Se21···Se13	3.785	3.813	3.867
d4	Se11···Se22	4.057	Se21···Se12	4.040	4.075	4.122
d5	Se12···Se14	3.823	Se22···Se24	3.888	3.873	3.936
d6	Se12···Se24	3.856	Se22···Se14	3.817	3.879	3.944
			2. Interstack			
d7	Se11···Se24	3.718[d]	Se21···Se14	3.713	3.752	3.847
d8	Se14···Se24	3.837	Se24···Se14	3.837	3.879	3.985
d9	Se12···Se12	3.618	Se22···Se22	3.571	3.639	3.741
d10	Se14···Se22	4.158	Se24···Se12	4.180	4.207	4.201

C. Average Local Se···Se Distance[e]

label[a]	20 K	125 K	298 K
d_{a1}	3.872	3.929	3.994
d_{a2}	3.942	3.929	3.994
d_{b1}	3.895	3.922	3.978
d_{b2}	3.881	3.922	3.978
d_{c1}	3.904	3.946	4.011
d_{c2}	3.910	3.946	4.011

[a] All of the labels given in this table are illustrated in Figure 3. [b] Note that above T_{AO}, D1 = D3. The least-squares planes for TMTSF molecules A1 and B1, as defined by the central tetraselenafulvalene region, C_6Se_4 (see illustration 1 below), are included in Supplementary Material. [c] At 20 K, there is a 0.4° dihedral angle between the central planar regions of TMTSF molecules A1 and B1, so that the interplanar separation of 3.54 Å is an approximae value. [d] Estimated standard deviations for Se···Se distances are as follows: ±0.002 to 0.003 Å at 20 K; ±0.001 Å at 125 K; ±0.001 Å at 298 K.

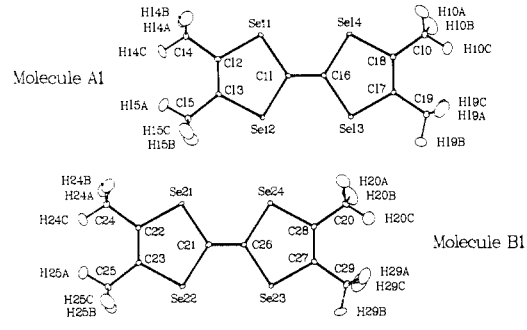

[e] The average Se···Se contacts within a stack, which are grouped according to contributions from Se11 and Se13 or from Se12 and Se14 (see illustration 1 above), are as follows: $d_{a1} = (d_1 + d_2 + d_5)/3$ between molecules A1 and A2; $d_{a2} = (d_1 + d_2 + d_5)/3$ between molecules B1 and B2; $d_{b1} = (d_3 + d_4 + d_6)/3$ between molecules A1 and B1; $d_{b2} = (d_3 + d_4 + d_6)/3$ between molecules A2 and B2. The average Se···Se contacts between stacks are as follows: $d_{c1} = (d_7 + d_8 + d_{10})/3$ between molecules A1 and B1′; $d_{c2} = (d_7 + d_8 + d_{10})/3$ between molecules A1 and B1′. Note that above T_{AO}, $d_{a1} = d_{a2}$, $d_{b1} = d_{b2}$, and $d_{c1} = d_{c2}$.

Figure 5 (parts a and b) show the HOMO bands of $(TMTSF)_2BF_4$ calculated for the 125 and 20 K structures, respectively. These bands are almost exclusively derived from the HOMO's of TMTSF molecules, and the contribution of the BF_4^- anion orbitals to the HOMO bands is practically zero. Because $(TMTSF)_2BF_4$ contains two and four TMTSF molecules per unit cell at 125 and 20 K, respectively, there are two and four HOMO sub bands in Figure 5 (parts a and b), respectively. Since there are three electrons per $(TMTSF)_2^+$ unit, the upper band of Figure 5a is half-filled. The intersection of the upper band and the Fermi level (i.e., the highest occupied band level) is along the intrastack direction $\Gamma \rightarrow X$ but not along the interstack direction $\Gamma \rightarrow Y$. Therefore, $(TMTSF)_2BF_4$ is a pseudo one-dimensional metal above the AO transition temperature, as in Figure 5a. With six electrons per $(TMTSF)_4^{2+}$ unit, the bottom three bands of Figure 5b are completely filled, and a band gap (~0.1 eV) exists between the third and the fourth bands. Thus, $(TMTSF)_2BF_4$ is a semiconductor below the AO transition temperature. According to Figure 5, the lattice dimerization, which accompanies the anion ordering at around 40 K, creates a band gap at the Fermi level. Consequently, the metal–insulator phase transition of $(TMTSF)_2BF_4$ is driven by two factors that aid in stabilizing the low temperature phase, namely, the donor–anion interactions (i.e., C–H···F) and the band gap opening. Finally, it is observed from Figure 5 that the HOMO band dispersion along the interstack direction $\Gamma \rightarrow Y$ is significant above 40 K but practically nonexistent below 40 K. That is, interactions *between* TMTSF stacks are greatly reduced below the metal–insulator transition temperature.

Concluding Remarks

The nature of the metal–insulator transition of $(TMTSF)_2BF_4$ at ~40 K was examined by determining its crystal structure at 20 K from single crystal neutron diffraction data. This study allowed us to accurately determine the H atom positions of the TMTSF methyl groups. Below ~40 K, each BF_4^- anion is ordered in such a way that only three of the four F atoms make short H···F contacts with the methyl group H atoms of four surrounding TMTSF molecules and that one short Se···F contact is maintained. Due to the anisotropic nature of this anion ordering, two adjacent $(TMTSF)_2^+$ of a TMTSF stack become nonequivalent. Thus, it may be said that the anion ordering and the dimerization of the TMTSF stack are closely related in $(TMTSF)_2BF_4$.

Our tight binding band calculations for $(TMTSF)_2BF_4$ show that this salt is a semiconductor with a small band gap below 40 K, which is a consequence of a Peierls transition involving the half-filled band of $(TMTSF)_2BF_4$ above 40 K. The presence of a short Se···F contact, and many short H···F contacts for each BF_4^- anion, suggests that the donor–anion interactions in $(TMTSF)_2BF_4$ are significant. Nevertheless, the valence band of $(TMTSF)_2BF_4$ contains practically no contribution from the BF_4^- anion orbital. Thus, the metal insulator transition of $(TMTSF)_2BF_4$ at ~40 K is a consequence of two different energy lowering factors, the anisotropic anion ordering and the stack dimerization. In other words, shortening of the H···F contacts is expected to strengthen the Coulombic attractive interactions between the anions and donors, and the dimerization of each TMTSF stack lowers the electronic energy of the stack.

Acknowledgment. Research at Argonne National Laboratory is sponsored by the U.S. Department of Energy (DOE) under contract W-31-109-Eng-38. The neutron diffraction measurements were carried out at the High Flux Beam Reactor (HFBR) at Brookhaven National Laboratory, Upton, NY 11973, which is operated under contract DE-AC02-76CH00016 with the DOE. We wish to thank J. Henriques for his expert technical assistance at the HFBR. Research at North Carolina State University was in part supported by the Dreyfus Foundation through a Camille and Henry Dreyfus Teacher-Scholar Award (1980-1985) to M.-H.W. which made it possible for M. E. to visit North Carolina

(45) Clementi, E.; Roetti, C. *At. Data Nucl. Data Tables* **1974**, *14*, 177.
(46) Ammeter, J. H.; Bürgi, H. B.; Thibeault, J. C.; Hoffman, R. *J. Am. Chem. Soc.* **1978**, *100*, 3686.
(47) (a) Peierls, R. E. *Quantum Theory for Solids*; Oxford University Press: London, 1955; p 108. (b) Whangbo, M.-H. *Acc. Chem. Res.* **1983**, *16*, 95. (c) Berlinsky, A. J. *Contemp. Phys.* **1976**, *17*, 331.
(48) Johnson, C. K. Report ORNL (U.S.), 1976; ORNL-5138, Oak Ridge National Laboratory, Oak Ridge, TN.

State University. The authors express their appreciation for computing time on the ER-Cray X-MP computer, made available by the DOE.

Registry No. $(TMTSF)_2BF_4$, 73731-79-0; neutron, 12586-31-1.

Supplementary Material Available: Tables S1-S3—positional and anisotropic thermal parameters of all atoms (20, 125, and 298 K); Table S4—some least-squares planes (20, 125, and 298 K) (6 pages); Tables S5 and S6—observed and calculated structure factors for the 20 K neutron data collected after slow cooling and fast cooling, respectively, of the $(TMTSF)_2BF_4$ crystal (20 pages). Ordering information is given on any current masthead page.

Synthesis, Characterization, and Reactivity of the (η^2-Acetone)pentaammineosmium(II) Complex

W. Dean Harman, David P. Fairlie, and Henry Taube*

Contribution from the Department of Chemistry, Stanford University, Stanford, California 94305. *Received May 29, 1985. Revised Manuscript Received July 25, 1986*

Abstract: When $[Os(NH_3)_5(CF_3SO_3)]^{2+}$ is reduced in acetone a novel (η^2-acetone)pentaammine complex is formed which shows markedly different reactivity from the ruthenium analogue. The crystal structure has been determined and C-O, Os-O, and Os-C bond lengths are found to be 1.32, 2.06, and 2.13 Å, respectively. The ν(C-O) has been assigned by isotopic labeling to be 1330 cm^{-1}.

A major interest in the chemistry of ruthenium(II) and osmium(II) pentaammines has been in their high affinity for π-acid ligands.[1] Although this effect is more dramatic in osmium,[2] the development of this chemistry has been hampered by the instability of osmium(II) pentaammine complexes in aqueous media.[3]

In our search for a convenient precursor to (π-acid)pentaammineosmium(II) complexes, we have investigated the reduction of $[Os(NH_3)_5(CF_3SO_3)](CF_3SO_3)_2$ in acetone. Instead of the labile ruthenium analogue we had expected,[4] we isolated a product that resists reaction with water, is stable at elevated temperatures, and is very slow to undergo substitution by stronger π-acids such as CO and isonicotinamide. This product has been characterized as $[Os(NH_3)_5((CH_3)_2CO)]^{2+}$ (I). The complex has the unusual structural feature that the acetone is bound to the metal through both carbon and oxygen. η^2-bound aldehydes and ketones have been observed in relatively few organometallic compounds,[5,6] and in most cases the aldehyde or ketone contains electron-withdrawing groups.

Here we describe the characterization and structure determination of this novel complex and include a brief discussion of its reactivity.

Experimental Section

Reagents. $[Os^{III}(NH_3)_5(TFMS)](TFMS)_2$ (TFMS = $CF_3SO_3^-$) was synthesized as described by Lay et al.[7] The acetone was purified by vacuum distillation over B_2O_3,[8] Et_2O by distillation over Na^0 and benzophenone, and MeOH by distillation over $Mg(MeO)_2$ prepared in situ by Mn^0 and I_2 under agron.[9] Bis(triphenylphosphoranylidene)ammonium chloride (PPNCl) (Aldrich Chemical Co.) and $H_2{}^{18}O$ (Stohler/KOR) were used without further purification. All solvents were thoroughly deoxygenated by purging with argon. All reactions were carried out under argon atmosphere in a Vacuum Atmospheres Corp. glovebox.

Table I. Crystal and Diffractometer Data for $[OsA_5(CH_3)_2CO]Cl_2$

empirical formula	$Os_1Cl_2O_1N_5C_3$
color of crystal	orange
space group	*Pbca*
cell dimensions, Å	
a	9.501 (5)
b	10.039 (6)
c	25.19 (3)
Z	8
V, Å^3	2404 (3)
calcd density, g/cm^3	2.23
mol wt	404.3
limits of data collection, deg	
2θ min	2
2θ max	55
unique reflns	3158
refln with $F_o > 3\sigma$	1753
R	0.055
R_w	0.064
absorption correction	yes
μ, cm^{-1}	110.488

Infrared spectra were recorded on an IBM 98 FTIR spectrometer. ^{13}C and ^1H NMR spectra were recorded on a Varian XL-400 spectrometer.[10] Electrochemical experiments were performed on a PAR Model 173 potentiostat which was driven by a PAR Model 175 universal programmer. Cyclic voltammograms were taken with a gold working electrode (3 mm^2), a platinum counter electrode, and a silver wire reference which was calibrated with the ferrocene/ferrocenium couple kept in situ. The peak-to-peak separation for this couple was ca. 60 mV for all cyclic voltammograms reported. Cyclic voltammograms taken at fast scan rates (1-500 V/s) were recorded on a Tektronix single-beam storage oscilloscope.

The measurements required for the calculation of the equilibrium constant were performed with use of modified rotated disk technique in

(1) Taube, H. *Pure Appl. Cem.* **1979**, *51*, 901-912.
(2) Reference 1, p 901.
(3) Reference 1, p 903.
(4) Baumann, J. A.; Meyer, T. J. *Inorg. Chem.* **1980**, *19*, 345-350.
(5) (a) Countryman, R.; Penfold, B. R. *Chem. Commun.* **1971**, 1598. Countryman, R.; Penfold, B. R. *J. Cryst. Mol. Struct.* **1972**, *2*, 281. (b) Ittel, S. D. *J. Organomet. Chem.* **1977**, *137*, 223. Ittel, S. D.; Ibers, J. A. *Adv. Organomet. Chem.* **1976**, *14*, 33. (c) Tsou, T. T.; Huffman, J. C.; Kochi, J. K. *Inorg. Chem.* **1979**, *18*, 2311-2317. (d) Wood, C. D.; Schrock, R. R. *J. Am. Chem. Soc.* **1979**, *101*, 5421. (e) Clark, G. R.; Headfold, C. E. L.; Marsden, K., Roper, W. R. *J. Organomet. Chem.* **1982**, *231*, 335-360. (f) Suggs, J. W.; Wovkulich, M. J. *Organometallics* **1985**, *4*, 1101-1107. (g) Gambarotta, S.; Floriani, C.; Chiesi-Villa, A.; Guastini, C. *J. Am. Chem. Soc.* **1985**, *107*, 2985-2986. (h) Kropp, K.; Skibbe, V.; Erker, G.; Krüger, C. *J. Am. Chem. Soc.* **1983**, *105*, 3353. (i) Brunner, H.; Wachter, J.; Bernal, I.; Creswick, M. *Angew. Chem., Inter. Ed. Engl.* **1979**, *18*, 861. (j) Berke, H.; Bankhardt, W.; Huttner, G.; Seyerl, J. v.; Zsolnai, L. *Chem. Ber.* **1981**, *114*, 2754.
(6) Avery, N. R.; Weinberg, W. H.; Anton, A. B.; Toby, B. H. *Phys. Rev. Lett.* **1983**, *51*, 682.
(7) Lay, P.; Magnuson, R.; Sen, J.; Taube, H. *J. Am. Chem. Soc.* **1982**, *104*, 7658.
(8) Burfield, D. R.; Smithers, R. H. *J. Org. Chem.* **1978**, *43* (*20*), 3966.
(9) Perrin, D. D.; Armarego, W. L. F.; Perrin, D. R. *Purification of Laboratory Chemicals*; Oxford: New York, 1980.
(10) All NMR spectra are presented in ppm shift from tetramethylsilane.

0002-7863/86/1508-8223$01.50/0